In-plane 2D focusing of surface waves by ultrathin refractive structures

Article *in* Optics Letters · November 2014

DOI: 10.1364/OL.39.006391

CITATIONS
22

READS
104

7 authors, including:

Angelo Angelini
INRIM Istituto Nazionale di Ricerca Metrologica
56 PUBLICATIONS **581** CITATIONS
SEE PROFILE

Andrea Lamberti
Politecnico di Torino
116 PUBLICATIONS **3,251** CITATIONS
SEE PROFILE

Serena Ricciardi
DiaSorin
29 PUBLICATIONS **496** CITATIONS
SEE PROFILE

Francesca Frascella
Politecnico di Torino
84 PUBLICATIONS **1,032** CITATIONS
SEE PROFILE

In-plane 2D focusing of surface waves by ultrathin refractive structures

A. Angelini,[1,2] A. Lamberti,[1] S. Ricciardi,[1] F. Frascella,[1] P. Munzert,[3] N. De Leo,[2] and E. Descrovi[1,*]

[1]*Department of Applied Science and Technology—DISAT, Politecnico di Torino, Torino I-10129, Italy*

[2]*Nanofacility Piemonte, Istituto Nazionale di Ricerca Metrologica—INRIM, Torino I-10135, Italy*

[3]*Fraunhofer Institute for Applied Optics and Precision Engineering—IOF, Jena D-07745, Germany*

**Corresponding author: emiliano.descrovi@polito.it*

Received September 8, 2014; accepted September 29, 2014;
posted October 10, 2014 (Doc. ID 222559); published November 4, 2014

In an attempt to provide a fully dielectric platform for two-dimensional optical circuitry, we report on the focusing features of an ultrathin polymeric lens fabricated on a planar multilayer. The radiation coupled to surface modes sustained by the multilayer can be focused or waveguide-injected into linear ridges by exploiting a dielectric-loading mechanism successfully exploited for plasmons. The low losses of this photonic system also allow long propagation lengths in the visible spectral range. Experimental observations made by fluorescence imaging of the multilayer surface are well supported by computational data obtained through an effective index approach. © 2014 Optical Society of America

OCIS codes: (240.0240) Optics at surfaces; (240.0310) Thin films; (240.6690) Surface waves; (350.3950) Micro-optics; (350.4238) Nanophotonics and photonic crystals.

http://dx.doi.org/10.1364/OL.39.006391

Recently, planar dielectric multilayers sustaining surface modes [1,2] (also called Bloch surface waves, BSWs) have gained popularity as an alternative platform to plasmonic metallic thin films in a number of applications, including sensing [3–8]. BSWs are characterized by an enhanced density of electromagnetic state close to the multilayer surface and well-defined dispersion relation and polarization state. Since BSWs lie beyond the light line and within the forbidden band of the multilayer, the wavevector component normal to the surface is complex. This leads to a generally attenuated field amplitude envelope from the multilayer surface to the outside and the inside of the multilayer. In this respect, BSWs can be seen as a photonic counterpart of surface plasmon polaritons (SPPs). There are several advantages in using BSW for sensing applications, such as the very low absorption losses exhibited by typical dielectric materials (e.g., silicon alloys [9], titania [10], tantalia [11], and also polymers [12]), a high degree of spectral and polarization tunability of surface resonances [13], a generally high Q-factor, and a corresponding strong field enhancement produced at the multilayer surface [14,15], giving an effective advantage in sensing applications when compared to typical ridge waveguide sensors, whose sensitivity is limited by the burial of the guided mode inside the high index layer [16].

Similar to surface plasmons on flat and structured films [17–23], BSWs can be manipulated by means of refractive or diffractive structures exploiting the BSW effective index shift due to the dielectric-loading effect. For example, BSWs can be confined and guided for tens to hundreds of micrometers [24–26], reflected [27], refracted [28], in-plane diffracted, and out-coupled from the surface [29].

In this work, we experimentally demonstrate the focusing capabilities of ultrathin refractive elements on a dielectric multilayer (also called a one-dimensional photonic crystal, 1DPC) designed for sustaining TE-polarized BSWs. In a recent work, it was shown that polymeric lenses fabricated on top of a 1DPC sustaining BSWs in the NIR can be used for focusing BSW on a polymer-coated region of the multilayer [30]. In the present case, we manage to employ individual ultrathin polymeric elements (30-nm thickness) for providing BSW focusing directly on the bare multilayer surface and BSW injection into a thin waveguide. In addition, we demonstrate that BSW focusing can indeed be detected in far field through straightforward fluorescence-based observations.

Here we make use of a 1DPC sustaining BSWs in the visible regime. A sketch of the photonic structure is shown in Fig. 1(a). The multilayer consists of four pairs of SiO_2 ($n = 1.45 + i2e-4$) and Ta_2O_5 ($n = 2.1 + i2e-4$) bilayers deposited on a glass coverslip. The Ta_2O_5 layers are 70-nm thick, while the SiO_2 layers are 210-nm thick, except for the last layer, which is 180-nm thick. On top of the surface we fabricated refractive structures such as lenses and waveguides. Such elements were fabricated by direct laser writing of 1-μm thick positive photoresist followed by a plasma-deposited polystyrene (PPST, $n = 1.55$) and a subsequent lift-off in acetone [30].

Here, BSWs exist in the visible spectral range. This is shown in the calculated reflectivity map for the TE polarization presented in Fig. 1(b). Incident light is provided from the glass substrate, to mimic a Kretschmann configuration for illumination. For each wavelength λ, the BSW dispersion has a specific normalized wavevector component parallel to the multilayer surface k_T/k_0, as identified by the narrow low-reflectivity region running beyond the light line. When a thin layer of additional material is deposited on the multilayer surface, a red shift of the BSW resonance is produced, leading to an increase of the effective index of the surface mode at fixed wavelength [23]. In Fig. 1(b) the BSW dispersion corresponding to the 1DPC coated with a 30-nm-thick polystyrene layer is also presented as a dashed black line. At $\lambda = 532$ nm, BSWs on bare and coated multilayer have

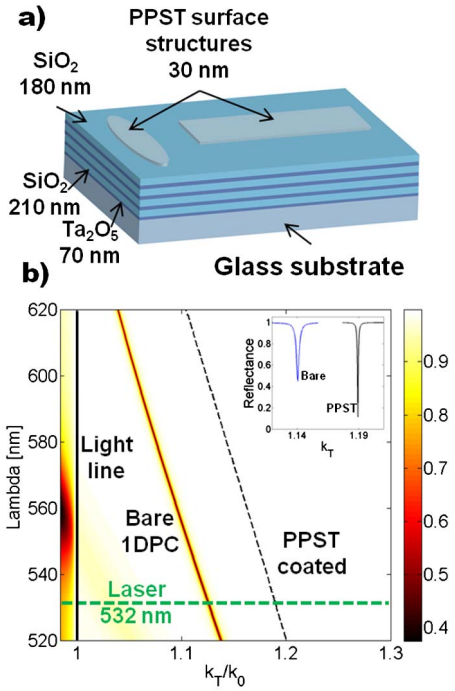

Fig. 1. (a) Sketch of the SiO_2-Ta_2O_5 multilayer hosting the polymeric refractive structures on the surface; (b) calculated reflectivity map for TE polarization showing the BSW dispersion on a bare multilayer. The BSW dispersion on a multilayer coated with a 30-nm-thick homogeneous layer of polystyrene is also illustrated (dashed line). The inset shows the two resonance angular profiles at $\lambda = 532$ nm.

a calculated effective index equal to 1.14 and 1.19, respectively (see inset).

The experimental setup is shown in Fig. 2. The back side of the glass substrate hosting the multilayer is oil contacted to a glass prism, according to the Kretschmann configuration. A doubled frequency Nd:YAG CW laser beam impinges on the 1DPC through the prism. The lateral size and the divergence of the beam can be adjusted by means of a beam expander system and a diaphragm. The angle of incidence θ_{BSW} is such that the transverse wavevector k_T of BSW at $\lambda = 532$ nm can be matched through the relationship $k_T = n_{prism} \cdot \sin \theta_{BSW}$, where n_{prism} is the glass-prism refractive index.

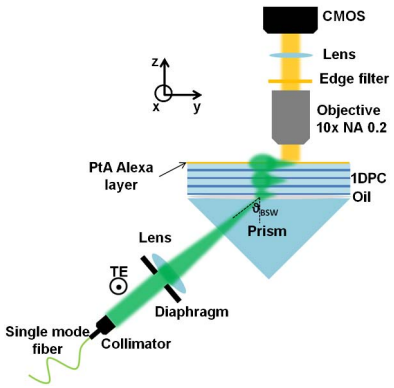

Fig. 2. Sketch of the experimental setup for BSW coupling in the Kretschmann configuration and fluorescence imaging of the planar multilayer.

In order to observe the intensity distribution of BSW on the surface of the 1DPC, one can directly collect the evanescent field by means of a near-field probe [29]. Although this method provides the amplitude and phase distribution of the field on the surface, it is time consuming and requires a dedicated apparatus. As a feasible alternative, it is possible to make the multilayer surface fluorescent upon excitation at BSW wavelengths. In this case, a fluorescence trace of the underlying excitation field can be obtained, thus revealing the BSW spatial distribution. Here, we incubated protein A conjugated with Alexa Fluor 546 (PtA-Alexa) on the multilayer surface for 20 min and then rinsed with phosphate buffered saline (PBS) buffer, so that an homogeneous and stable fluorescent layer is obtained. The dielectric loading effect played by such a monolayer is negligible here, since the slightly red-shifted BSW resonance [8] still falls within the angular divergence of the weakly focused incident laser beam. In this way, fluorophores act as a probe for the BSW near-field intensity, thus allowing a simple fluorescence imaging from the air side with a CMOS camera. One drawback of this approach is represented by the absorption introduced by the presence of the fluorophores on the surface. As a result, the overall losses of BSW slightly increase and the propagation length decreases from the expected value of 34 μm (as calculated through the full width at half-maximum [FWHM] of the calculated resonance [31]) to about 20 μm (data not shown).

The calculated effective indices of BSW at $\lambda = 532$ nm have been used to model the BSW propagation and focusing in a 2D effective index model built on commercial software (COMSOL 4.2a RF module). However, in order to provide a realistic comparison with measurements, absorption introduced by the ptA-Alexa layer should also be considered. Upon introducing a fictitious absorption coefficient as high as $1.8 \cdot 10^{-3}$ the 2D model provides a BSW propagating with a propagation length of 20 μm, as experimentally observed. We point out that the absorption coefficient used in the 2D model is not representative of the specific absorption for each of the 1DPC layers.

The planar lens is a biconvex lens with a radius of curvature of 6 μm and a diameter of 10.4 μm. The expected focal plane is located at about 35 μm from the lens. From the 2D effective index model, the BSW is focused according to an intensity distribution as illustrated in Fig. 3(a). Experimentally, the BSW focusing effect produced by the 30-nm-thick polymeric lens is observed as shown in Fig. 3(b). This fluorescence image is rendered in false colors to help a direct comparison with calculations in Fig. 3(a). The dominant role of losses is such that the intensity enhancement due to BSW focusing cannot be appreciated.

In order to appreciate the good agreement between experiment and calculation, the cross-sectional intensity distribution in the focal region (about 35 μm far from the center of the lens) are considered.

The calculated FWHM of the intensity distribution on the focal plane is about 2 μm. For comparison purposes, the limited spatial resolution of the collection optics needs to be taken into account. To this aim, we convolved the calculated profile with a Gaussian function

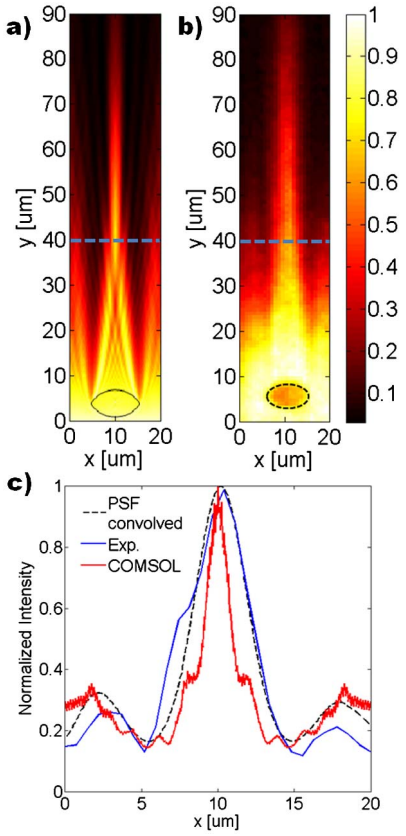

Fig. 3. (a) Calculated BSW focusing by means of a 30-nm-thick lens having a radius of curvature of 6 μm and diameter 10.4 μm. (b) Fluorescence image of BSW as focused by the polymeric lens (marked with the black dashed line). The blue dashed lines indicate the focal plane. (c) Calculated (solid red line) and measured (solid blue line) transverse intensity profiles in the focal planes. The black dashed line is obtained by convolving the calculated profile with an approximate point spread function (PSF) associated with the collection optics.

(roughly mimicking the point spread function (PSF) of the collection objective) whose variance is given by the Rayleigh resolution limit: $\sigma^2 = \lambda/(2\ \mathrm{NA}) = 1.43$ μm, where $\lambda = 570$ nm is the peak fluorescence emission wavelength and NA $= 0.2$ is the numerical aperture of the collection objective. After convolution we obtained a calculated field-intensity profile having a FWHM $=$ 4.3 μm, which is close to the corresponding measured profile having a FWHM $= 5 \pm 1$ μm. The accuracy of this estimation is limited by the image pixelization of the CMOS camera. The as-measured and the convolved calculated profiles are in very good agreement, as shown in Fig. 3(c). We finally observe that the thin lens on the multilayer surface appears rather dark in the fluorescence image because of the antifouling feature of PPST [32], whereby fewer PtA-Alexa molecules can be grafted thereon.

Two-dimensional refractive elements can serve as waveguide couplers. We positioned a lens in front of a thin planar ridge whose terminal end is approximately within the focal plane of the lens. The lens is identical to the previous one. The rectangular PPST waveguide is 100-μm long, 5-μm wide, and 30-nm thick and is made of PPST, as is the lens. Computational results show that the BSW, focused by the lens, is actually injected into the

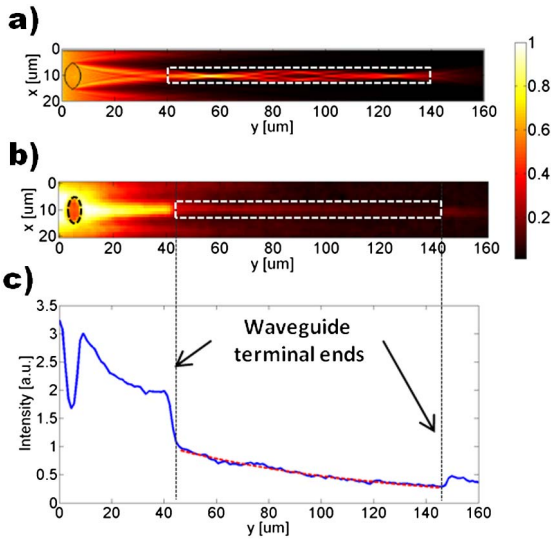

Fig. 4. (a) Calculated and (b) measured intensity distribution of a BSW injected into a polymeric ridge waveguide (contour, dashed white line) by means of a 2D lens. (c) Experimental intensity profile along the y axis extracted from (b). The vertical dotted lines indicate the waveguide terminal ends. Inside the waveguide the profile is well fitted by an exponentially decaying function (dashed red line).

ridge and propagates along the waveguide [Fig. 4(a)]. The experimental observation presented in Fig. 4(b) confirms that an effective index variation produced by a 30-nm PPST layer is high enough to guide the BSW in a straight direction.

Similar to Fig. 3(b), the drastic reduction of fluorescence intensity observed on the waveguide is due to a lower concentration of ptA Alexa adsorbed on the PPST structure. If a longitudinal cross-sectional profile of intensity is considered [Fig. 4(c)], the sharp changes in the ptA-Alexa concentration adsorbed on the surface can be appreciated at both terminal ends of the ridge, as indicated. Within the waveguide, the intensity distribution (integrated along the x axis in a region between 9 and 11 μm) has an exponentially decaying profile. In order to calculate the decay constant, we fit the experimental profile with a function $I(y) = I_0 \cdot \exp(-y/L)$, where I_0 is the initial intensity at the beginning of the guide and L is the decay length of the guided BSW. Best fit is obtained for $L = 83.3$ μm, which is roughly four times larger than the propagation length observed outside the guide. This value agrees well with the theoretical value of 83.7 μm as expected on a uniform 30-nm-thick PPST layer. In this case, the absorption due to fluorescent probes has minor impact due to antifouling properties of PPST. Furthermore, the increased decay length is probably due to the narrower resonance in the presence of the PPST additional layer (see inset in Fig. 1). In the effective medium model, upon a proper scaling down of the absorption coefficient in the waveguide by a factor of four (leading to an absorption coefficient of $4.38 \cdot 10^{-4}$), we find a good matching between calculations and experiment [see Figs. 4(a) and 4(b)].

In conclusion, we demonstrated the capabilities of ultrathin polymeric elements ($\lambda/18$ thickness) to focus surface modes on planar multilayers. Thanks to a

dielectric-loading mechanism, which is well-known for surface plasmons, we managed to manipulate BSW in a controlled way by refractive elements. Although negatively affected by the presence of absorbing fluorophores, the propagation length of BSWs is large enough to allow the development of complex two-dimensional surface photonic circuitry, even in the visible range.

Such results make BSWs suitable for surface photonic circuits in addition to sensing applications, mainly because of the large propagation lengths that can be achieved. Performance can be eventually enhanced by employing highly transparent materials or eventually by suppressing the leakage radiation increasing the number of layers in the multilayer structure [29].

This research was funded by the Italian Flagship Project NANOMAX (MIUR PNR 2011–2013) and the EU project BILOBA (318035).

References

1. P. Yeh, A. Yariv, and C.-S. Hong, J. Opt. Soc. Am. **67**, 423 (1977).
2. W. M. Robertson, G. Arjavalingam, R. D. Meade, K. D. Brommer, A. M. Rappe, and J. D. Joannopoulos, Opt. Lett. **18**, 528 (1993).
3. A. Farmer, A. C. Friedli, S. M. Wright, and W. M. Robertson, Sens. Actuators B **173**, 79 (2012).
4. V. N. Konopsky and E. V. Alieva, Biosens. Bioelectron. **25**, 1212 (2010).
5. Y. Guo, J. Y. Ye, C. Divin, B. Huang, T. P. Thomas, J. R. Baker, and T. B. Norris, Anal. Chem. **82**, 5211 (2010).
6. F. Villa, L. E. Regalado, F. Ramos-Mendieta, J. Gaspar-Armenta, and T. Lopez-Ríos, Opt. Lett. **27**, 646 (2002).
7. F. Michelotti, B. Sciacca, L. Dominici, M. Quaglio, E. Descrovi, F. Giorgis, and F. Geobaldo, Phys. Chem. Chem. Phys. **12**, 502 (2010).
8. A. Sinibaldi, N. Danz, E. Descrovi, P. Munzert, U. Schulz, F. Sonntag, L. Dominici, and F. Michelotti, Sens. Actuators B **174**, 292 (2012).
9. R. Badugu, K. Nowazcyk, E. Descrovi, and J. R. Lakowicz, Anal. Biochem. **442**, 83 (2013).
10. V. Koju and W. Robertson, Opt. Express **22**, 15679 (2014).
11. F. Michelotti, A. Sinibaldi, N. Danz, P. Munzert, and E. Descrovi, Opt. Lett. **38**, 616 (2013).
12. L. Fornasari, F. Floris, M. Patrini, G. Canazza, G. Guizzetti, D. Comoretto, and F. Marabelli, Appl. Phys. Lett. **105**, 053303 (2014).
13. J. Gao, A. Sarangan, and Q. Zhan, Opt. Lett. **37**, 2640 (2012).
14. M. Ballarini, F. Frascella, F. Michelotti, G. Digregorio, P. Rivolo, V. Paeder, V. Musi, F. Giorgis, and E. Descrovi, Appl. Phys. Lett. **99**, 043302 (2011).
15. A. Delfan, M. Liscidini, and J. E. Sipe, J. Opt. Soc. Am. B **29**, 1863 (2012).
16. A. Densmore, D. X. Xu, S. Janz, P. Waldron, J. Lapointe, T. Mischki, G. Lopinski, A. Delâge, J. H. Schmid, and P. Cheben, Adv. Opt. Technol. **2008**, 725967 (2008).
17. Z. Liu, J. M. Steele, W. Srituravanich, Y. Pikus, C. Sun, and X. Zhang, Nano Lett. **5**, 1726 (2005).
18. C. Zhao, Y. Liu, Y. Zhao, N. Fang, and T. J. Huang, Nat. Commun. **4**, 2305 (2013).
19. T. Zentgraf, Y. Liu, M. H. Mikkelsen, J. Valentine, and X. Zhang, Nat. Nanotechnol. **6**, 151 (2011).
20. G. M. Lerman, A. Yanai, and U. Levy, Nano Lett. **9**, 2139 (2009).
21. L. Li, T. Li, S. Wang, S. Zhu, and X. Zhang, Nano Lett. **11**, 4357 (2011).
22. D. G. Zhang, X. C. Yuan, J. Bu, G. H. Yuan, Q. Wang, J. Lin, X. J. Zhang, P. Wang, H. Ming, and T. Mei, Opt. Express **17**, 11315 (2009).
23. C. Zhao and J. Zhang, ACS Nano **4**, 6433 (2010).
24. T. Sfez, E. Descrovi, L. Yu, D. Brunazzo, M. Quaglio, L. Dominici, W. Nakagawa, F. Michelotti, F. Giorgis, O. J. F. Martin, and H. P. Herzig, J. Opt. Soc. Am. B **27**, 1617 (2010).
25. M. Ballarini, F. Frascella, E. Enrico, P. Mandracci, N. De Leo, F. Michelotti, F. Giorgis, and E. Descrovi, Appl. Phys. Lett. **100**, 063305 (2012).
26. M. Liscidini, D. Gerace, D. Sanvitto, and D. Bajoni, Appl. Phys. Lett. **98**, 121118 (2011).
27. E. Descrovi, F. Giorgis, L. Dominici, and F. Michelotti, Opt. Lett. **33**, 243 (2008).
28. T. Sfez, E. Descrovi, L. Yu, M. Quaglio, L. Dominici, W. Nakagawa, F. Michelotti, F. Giorgis, and H. P. Herzig, Appl. Phys. Lett. **96**, 151101 (2010).
29. A. Angelini, E. Barakat, P. Munzert, L. Boarino, N. De Leo, E. Enrico, F. Giorgis, H. P. Herzig, C. F. Pirri, and E. Descrovi, Sci. Rep. **4**, 5428 (2014).
30. L. Yu, E. Barakat, T. Sfez, L. Hvozdara, J. Di Francesco, and H. P. Herzig, Light Sci. Appl. **3**, e124 (2014).
31. R. Ulrich, J. Opt. Soc. Am. **60**, 1337 (1970).
32. M. Ballarini, F. Frascella, N. De Leo, S. Ricciardi, P. Rivolo, P. Mandracci, E. Enrico, F. Giorgis, F. Michelotti, and E. Descrovi, Opt. Express **20**, 6703 (2012).